ASME 2016 International Design Engineering Technical Conferences and Computers and Information in Engineering Conference IDETC2016
August 21-24, 2016, Charlotte, North Carolina

IDETC2016-60550

SOFT SPHERICAL TENSEGRITY ROBOT DESIGN USING ROD-CENTERED ACTUATION AND CONTROL

Lee-Huang Chen
Kyunam Kim
Ellande Tang
Kevin Li
Richard House
Alice M. Agogino
Mechanical Engineering
University of California, Berkeley

Adrian Agogino
University of California, Santa Cruz
Vytas Sunspiral
Stinger Ghaffarian Technologies
Intelligent Systems Division
NASA Ames Research Center
Mountain View, California USA

Erik Jung
Computer Engineering
University of California, Santa Cruz USA

ABSTRACT

This paper presents the design, analysis and testing of a fully actuated modular spherical tensegrity robot for co-robotic and space exploration applications. Robots built from tensegrity structures (composed of pure tensile and compression elements) have many potential benefits including high robustness through redundancy, many degrees of freedom in movement and flexible design. However to fully take advantage of these properties a significant fraction of the tensile elements should be active, leading to a potential increase in complexity, messy cable and power routing systems and increased design difficulty. Here we describe an elegant solution to a fully actuated tensegrity robot: The TT-3 (version 3) tensegrity robot, developed at UC Berkeley, in collaboration with NASA Ames, is a lightweight, low cost, modular, and rapidly prototyped spherical tensegrity robot. This robot is based on a ball-shaped six-bar tensegrity structure and features a unique modular rod-centered distributed actuation and control architecture.

This paper presents the novel mechanism design, architecture and simulations of TT-3, the first untethered, fully actuated cable-driven six-bar tensegrity spherical robot ever built and tested for mobility. Furthermore, this paper discusses the controls and preliminary testing performed to observe the system's behavior and performance.

INTRODUCTION

Buckminster Fuller coined the word "tensegrity" in 1962 as a portmanteau of "tensile integrity" [1]. Tensegrity structures consist primarily of compression elements (rods) and tension elements (cables). The rods/cables of the structure experience pure compression/tension under equilibrium conditions. Tensegrity structures do not experience bending moments, which give them the unique and beneficial characteristic of simplifying the design process and reducing the number of failure modes. The rods and cables are only required to withstand single axis loading [2].

Tensegrity structures exhibit compliant behavior from their ability to distribute external forces globally. With this compliant characteristic, tensegrities can be used as a platform for soft robotic designs. Tensegrity soft robots have the ability to ensure that they will not injure humans during co-robotic applications, a critical trait behind the increase popularity in soft robots.

Tensegrity structures are of interest in the field of soft robotics due to their flexible and robust nature. They have the ability to passively distribute forces globally providing shock protection from unexpected impact forces. This feature makes them a robust mobile platform suitable for uneven and unpredictable environments in which traditional robots struggle.

The unique properties of tensegrity robost make them well-suited for a new generation of robotic landers/rovers for space exploration. The ability to land an inexpensive rover without

damage and traverse uncertain territory is highly desirable for successful space exploration. In addition, the robot's intrinsic structural robustness allows it to handle or recover from unexpected and undesirable interactions with the environment (e.g., collision with obstacles) while moving. This could allow significantly faster science return as compared to current rover concepts that must meticulously plan every operation to provide adequate safety.

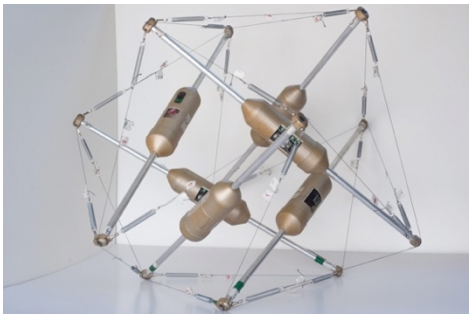

FIGURE 1. TT-3, A SIX-BAR SPHERICAL TENSEGRITY ROBOT.

The UC Berkeley Emergent Space Tensegrities Laboratory has been collaborating with the NASA Ames Research Center on using tensegrity structures as the basis for next generation space exploration systems. Traditionally, rigid wheeled robots, like the Mars Curiosity rover, have been the primary space exploration platform. Heavy rigid robots require detailed sensing during operation, while robust compliant robots like TT-3 can operate with minimal sensing at a fraction of the weight.

PRIOR RESEARCH

Prior work with tensegrity structures has focused on robust static structures in modern architecture, art and structural applications. Examples include Snelson's unique, stable biotensegrity art pieces [3], Tibert's deployable tensegrity space structures [4] and Fu's work on designing large-scale tensegrity domes [5]. However, only recently, in parallel with the rise of soft robotics, have tensegrities come to the forefront of robotic design.

In examining examples of work on active tensegrity structures, the number of examples grows fewer. Of note are NASA Ames Research Center's work on the Spherical Underactuated Planetary Exploration Robot ball (SUPERball) and its predecessor, the Reservoir Compliant Tensegrity Robot (ReCTeR) {6,7]. Both SUPERball and ReCTeR are untethered, spherical tensegrity robots capable of cable-actuated deformation and motion. Unlike our TT-3 robot, both SUPERball and ReCTeR are under actuated systems with 12 and 6 actuators, respectively.

The predecessor to the TT-3 (version 3) robot is the TT-2 (version 2) robot shown in Fig. 2, which is UC Berkeley's spherical tensegrity robot, featuring a similar six-bar tensegrity structure with 24 actuators. The six rigid members were constructed from balsa wood on the TT-1 (version 1) robot, eventually being upgraded to fiberglass struts on the TT-2 robot, while the tensional members were comprised of linear actuators in series with elastic cords [8]. Simulation work in NASA's Tensegrity Robotics Toolkit (NTRT) environment allowed for development of multi-actuator strategies to efficiently generate punctuated, or step-wise, rolling motion.

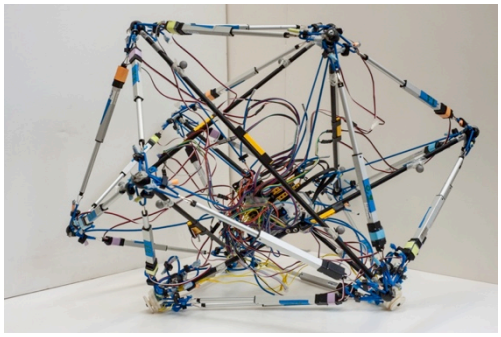

FIGURE 2. THE TT-2 TENSEGRITY ROBOT.

Apart from spherical tensegrity robots, spine-like tensegrity structures have also been explored as a locomotion strategy with work being done on cable-connected and cable-actuated spine vertebrate as well as a duct exploring robot with two tetrahedral frames linked by hinge joints and controlled with linear actuators [9,10,11,12]. EPFL's IMAC Laboratory has expandable tensegrities for dynamic use in rescue situations. Paul and Lipson have demonstrated gait production in a three-strut, nine-cable arrangement [13,14,15].

The dynamic, highly-specialized and non-standardized nature of tensegrity robotics has motivated the development of a rapid prototyping tensegrity system at UC Berkeley, in collaboration with NASA Ames. The development of TT-3 will help construct a modular hardware and controls framework for tensegrity-based robotic structures that will accelerate the research in this emerging field.

ROD-CENTERED DESIGN

The original target mission was the development of a lander/rover system that could explore Titan, the largest moon of Saturn. Some of the main design challenges are (1) a robot system that can sustain high-speed impact, (2) a robot that can maneuver around the surface of the planet after landing, (3) a robot that can carry scientific payload, (4) a robot that can transfer or absorb unexpected forces, (5) a low-cost, lightweight system. With these abilities, possible missions were expanded to include exploring the craters of Earth's moon.

With these target goals, tensegrity structures were predicted to be a good basis for a design platform as they have the ability to (1) distribute external forces globally, (2) high strength to weight ratio, (3) adjustable structure stiffness. The ability to distribute external forces throughout the structure means the structure has the potential to absorb large impact forces from different forms of landing phases in the mission. The characteristic of high strength to weight ratio provides the possibility to develop a lightweight system. Combining the

ability to distribute forces globally with stiffness adjustments, it is possible for the structure to change its shape by changing the tension levels at different segments of the structure. With the proper control of this shape-shifting characteristic, the structure can perform punctuated rolling, which will be discussed in more detail in later sections.

The middle point of the rod is the furthest location from the surface of the six-bar tensegrity. It is the location to best protect the critical components during rolling and dropping. Therefore, placement all the critical components (e.g., controllers and actuators) to the center of the rods can potentially improve the reliability and functionality of the system.

SIMULATION MODELING

For simulation we use NASA's Tensegrity Robotics Toolkit (NTRT) [16]. In simulation, the dynamics and kinematics of different designs can be explored, and inherent advantages and disadvantages of adjustments in parameters can be compared. The NTRT simulator has the ability to have rapid development structures in this physics-based environment. Since tensegrity structures have complex internal force distributions at different states, NTRT can be used as a tool to assist with designing tensegrity robots. With NTRT, a six-bar structure with known parameters, such as rod length, rod diameter, rod mass, and spring constant, can be modeled and its behavior simulated. With the modeled tensegrity, different pre-tension values can be applied to graphically visualize the appearance of the tensegrity structure.

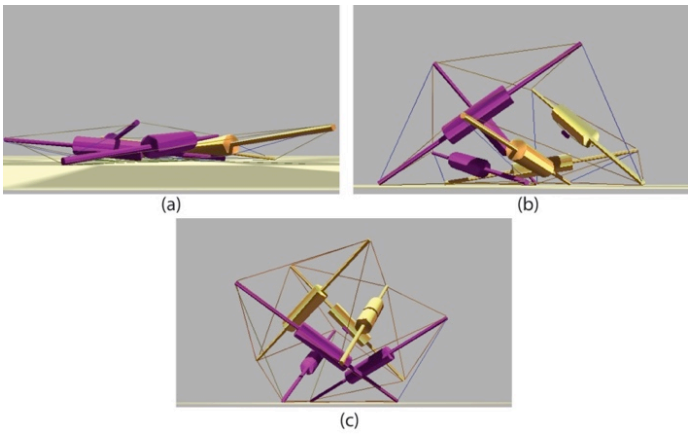

FIGURE 3. NTRT SIMULATIONS OF TT-3 WITH DIFFERENT PRE-TENTIONS. (a)(b)(c) IS THE SEQUENCE OF INCREASING PRE-TENSION.

Shown in Fig. 3, a model of TT-3 is applied with three different pre-tension values. With a small tension value, TT-3 appears to be flat on the ground. With increasing tension, the structure will gradually stand up to be more sphere-like. NTRT can estimate the required tension force for modeled structures. In the case of TT-3, the initial modeling of TT-3 with close estimation of system parameters shows the minimum tension required for the structure to be 17.5N to be sphere like. Knowing the potential tension requirement can help the designer better select critical components, such as the actuators, needed for the robot. This feature can greatly improve the efficiency of the design process and reduce the need for constant trial-and-error with designing physical prototypes.

IMPACT DYNAMICS

The compliant tensegrity structure has the ability to absorb forces during impact. This ability is due to the transfer of the energy throughout the system. During impact, the structure will deform; the deformation in the structure is the transfer of kinetic energy to the potential energy in the elastic element. For example, a tensegrity structure using extension springs as its elastic elements, the springs will stretch to a higher potential state during impact. This is the transfer of the impact energy to strain energy in springs. Therefore, it is potentially more valuable to have a structure that can be deformed more during impact.

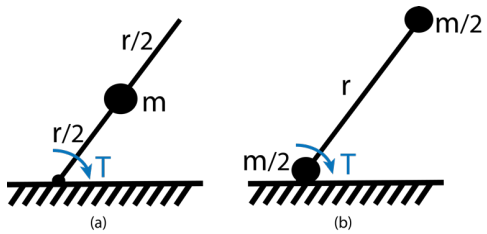

FIGURE 4. (a) A SINGLE ROD OF THE TENSEGRITY STRCTURE IS MODELED WITH A MASS AT THE CENTER OF THE ROD. (b) A SINGLE ROD OF THE TENSEGRITY STRUCTURE IS MODEL WITH TWO HALF MASSES ON TWO ENDS OF THE ROD. IN THE FIGURES, M IS THE ROD MASS, R IS THE ROD LENGTH AND T IS THE TORQUE APPLIED.

A different rod design will result in different mass distributions across the rod, which in turn will affect the behavior of the rod upon impact. In order to see the differences two simple cases are presented in Fig. 4. In the first rod design, the rod mass is concentrated at its center (Fig. 4(a)). Its mass moment of inertia with respect to the ground contact can be calculated with Eqn. 1.

$$I_A = m \cdot \left(\frac{r}{2}\right)^2 = m \cdot \frac{r^2}{4} \tag{1}$$

On the other hand, the second rod design divided the rod mass evenly on the two ends (Fig. 4(b)). In this case, the mass moment of inertia with respect to the ground contact can be calculated with Eqn. 2.

$$I_B = \frac{m}{2} \cdot r^2 \tag{2}$$

If each rod receives the same torque while the ground contact end is the pivot point, the different mass distribution will result in different angular acceleration shown in Eqn. 3.

$$T = I_A \cdot \alpha_A = I_B \cdot \alpha_B \tag{3}$$

$$I_A = \frac{I_B}{2} \tag{4}$$

$$\alpha_A = 2\alpha_B \tag{5}$$

The result is that the rod in Fig. 4(a) will have twice the angular acceleration of the rod in Fig. 4(b) shown in Eqn. 5. The higher angular acceleration of the rod is one of the main benefits of the rod-centered design because it implies the structure will deform more when the same torque is applied. The larger deformation in the structure means the displacement of the springs or the elastic elements in the structure will be larger.

IMPACT SIMULATION

NTRT simulations were performed to confirm the difference in behavior of the rods presented in Fig. 4 at the structural level during impact. From the previous section, the structure with mass at the center of the rod should be more compliant than the structure with its mass evenly divided at the two ends of the rod. This means the structure with its mass at the center of the rod should deform more than the other structure.

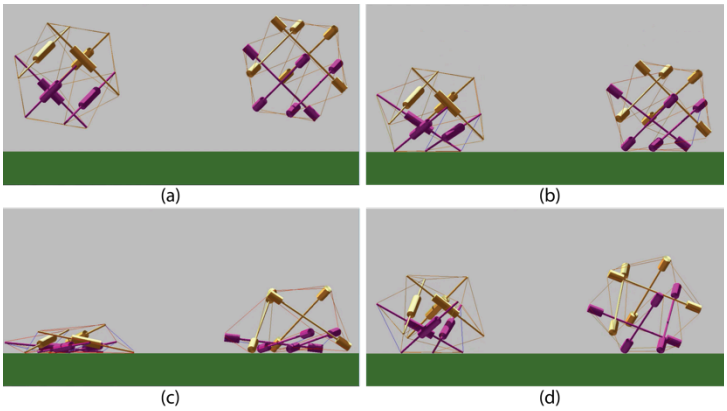

FIGURE 5. (a)(b)(c)(d) IS THE SEQUENCE OF IMPACT FROM THE SAME HEIGHT OF TWO TENSEGRITY STRUCTURES WITH DIFFERENT MASS DISTRIBUTION.

Figure 5 shows the sequence of both tensegrity structures with different mass distributions impacting the ground from the same height. All parameters of the two structures are the same except the location of the mass. The structure on the left in Fig. 5 has a large mass at the center of the rod, and the structure on the right has the same large mass but it is divided to the two ends of the rod. This simulation and resulting images (Fig. 5) confirm the structure on the left is able to deform more during impact.

HARDWARE DESIGN

The previous sections have shown the benefits of locating the majority of the mass of the system at the center of the rod; therefore, the rod-centered design will be the base architecture of the TT-3 robot design.

The goal of the project is to create a robot that can absorb the energy from landing and be actuated to perform locomotion. It is also important to design a robot that can maneuver around various terrains. It is shown in the later sections that one mode of locomotion for tensegrity robots is to shift its center of mass outside of the base triangle to perform a punctuated roll.

An actuated cable in series with a spring is the chosen method for changing the shape of the structure to adjust the location of the projected center of mass. Cable actuation is chosen due to its ability to have long displacements between the nodes of the tensegrity robot. The range of displacement between the nodes of the structure can greatly determine the potential of shape shifting.

A simple motor and spool design is the selected method to change the length of cable between the nodes of the structure. This method allows for the ease of placement of the motor at a desired location, which is the center of the rod for TT-3.

Actuator Selection

After performing the required force simulation from NTRT, a few motors were selected for potential actuators for the robot. One key criterion during actuator selection was the high torque to weight ratio. High torque to weight ratio creates the possibility to develop a lightweight tensegrity robot with a large range of tension adjustments and stiffness.

Three motors were selected: Pololu model 1595, Pololu model 2275, and Pololu 2218. They are all brushed DC motors because low cost is a goal for the overall system. The Pololu motor model 1595 weights 10.5g. The Pololu motor model 2275 weights 103g. And the Pololu motor model 2218 weights 9.5g. Pololu 2218 and 1595 are both very lightweight, making them highly useful as there will be 24 motors needed to construct a fully actuated robot.

Actuator Testing

The selected motors were tested with the EXTECH heavy-duty digital torque meter to measure the stall. The motors were secured on a fixer, and voltage was supplied to the motors individually. The supply voltage was started with one volt, and then increased with the increment of one up to 9 volts. At each voltage, the stall torque value was recorded. This process was used to observe the behavior of the motors at different voltages, and was used to compare with the manufacturer specification. Pololu 2218 was the chosen actuator through this process. The other 2 actuators did not perform reliably under high voltage. The gears seem to skip under high torque conditions.

HARDWARE PROTOTYPE

Actuation Module using Acrylic Platform

The new design strategy was to design a modular actuation module that is located at the center of the rod. There are a total of 24 motors; six rods and 4 motors in each module. It is important to have a reliable and robust system for space exploration. Therefore, redundancy should be a key design feature. Therefore, TT-3 is designed with an individual microcontroller in its actuation module.

Wireless communication is used as the main method for command signals and data transfer. The use of wireless units greatly simplifies the wiring, and no wires are required between the rods.

For the first prototype, an acrylic sheet was used as the platform for mounting all the components for the actuation module. Most of components used were off-the-shelf, including a microcontroller, a wireless unit, a voltage regular, two motor drivers, four motors and a battery pack. The hole patterns on the acrylic board were first modeled on a computer-aided design (CAD) program, then the pattern was exported to a laser cutter for manufacturing. Shown in Fig. 6 is the top and bottom of the assembled acrylic actuation module.

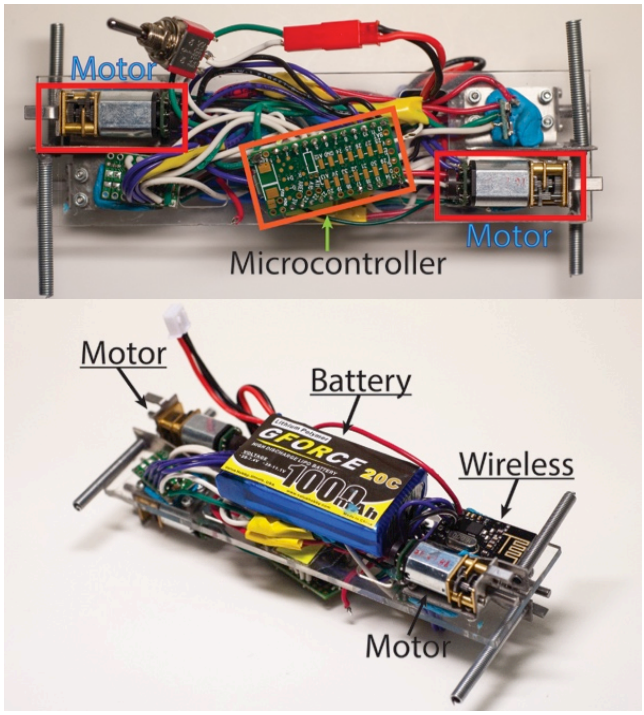

FIGURE 6. THE TOP AND BOTTOM OF THE ACRYLIC ACTUATION MODULE, WHICH INCLUDES 4 MOTORS, A MICROCONTROLLER, 1 WIRELESS UNIT, 2 MOTOR DRIVER, 1 VOLTAGE REGULAR, AND A BATTERY PACK.

An enclosure was designed to house the actuation module. The enclosure has an internal rail for the acrylic plate to slide into with a cap placed over the open end to fully enclose the actuation module. Currently, the gold colored enclosure shown in Figs. 7 and 8, is manufactured with a fused deposition modeling (FDM) machine. Two 0.5 inch diameter aluminum tubes are connected to both ends of the 3D-printed enclosure. One of the design features allows for the quick removal of the tubes, and the tube length can be adjusted for modularity. With different tube lengths, different sizes of tensegrity robots can be built, making the TT-3 platform modular and adjustable.

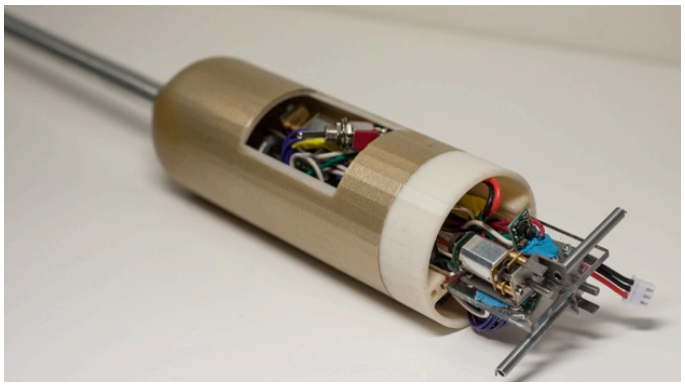

FIGURE 7. THE ACRYLIC ACTUATION MODULE SLIDES INTO THE PLASTIC ENCLOSURE.

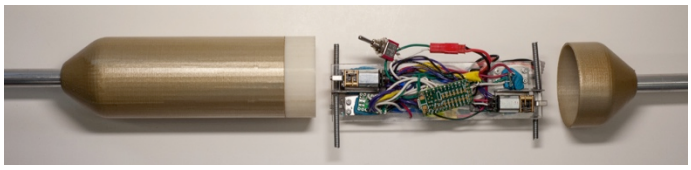

FIGURE 8. IMAGE SHOWS THE ALUMINUM TUBES, PLASTIC ENCLOSURE, ACRYLIC ACTUATION MODULE, AND ENCLOSURE CAP, WHICH CONSTRUCTS A ROD OF TT-3 ROBOT.

Actuation Module using Printed Circuit Board

The acrylic plastic prototyped actuation module design described previously was able to provide promising results during preliminary testing. The TT-3 built with the acrylic actuation module was able to perform punctuated rolling with only a single motor actuated. However, the robot experienced unreliability during testing of long durations. Sometimes, the slave module would power off during rolling. After performing a failure mode analysis, it was discovered that the complex wiring on the acrylic actuation module was causing the inconsistent connection. In addition to the unreliability of the wire connections, the acrylic actuation modules were difficult to reproduce, which make it less ideal as a rapid prototyped robot.

The solution for this issue was the use of a custom printed circuit boards as the replacement of the wires and acrylic support structure show in Fig. 9. The custom printed circuit board (PCB) as the base structure for building the actuation modules not only increased reliability, but also reduced the time and complexity of the prototyping process. The assembly time was reduced from 24 person-hours to eight person-hours for the full assembly of the six actuation modules.

Figure 10 shows how the printed circuit board actuation module is placed on TT-3, and how the cables are routed from

the motors out to the neighboring rod to form the six bar tensegrity structure.

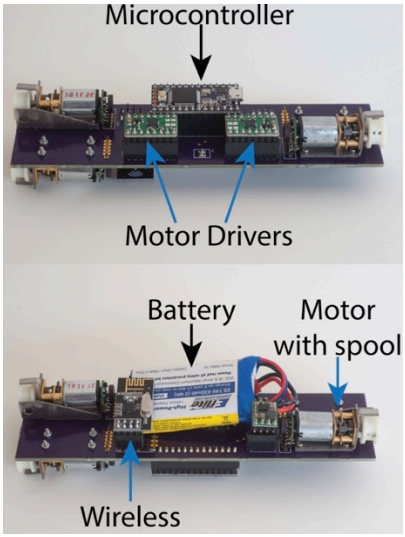

FIGURE 9. THIS IMAGE DISPLAYS THE TOP AND BOTTOM OF THE ACTUATION MODULE USING PRINTED CIRCUIT BOARD AS ITS BASE PLATFORM.

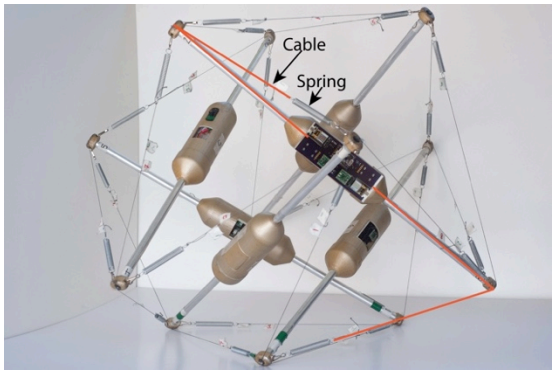

FIGURE 10. IMAGE DISPLAYING HOW THE CABLES ARE ROUTED FROM THE CENTER MODULE.

Endcap Design

Due to the relatively low power of the driving motors, any means of reducing cable friction in the robot will improve its functionality. For a cable driven robot, the cables might experience high friction while in contact with material with different velocities or routings through corners. In the TT-3 system, one of the main locations of high friction force is the point of contact where the cable is routed out of the rod to connect with the neighboring rod. To address this issue, several "endcaps" were designed to fit on the end of the compression members, which will provide various routing methods for the cables. In addition to friction force reduction, these endcaps also need to provide non-permanent connection points for the other two tension members that connect to the end of a compression member.

Direct Routing through Polished Aluminum Tubes

Shown in Fig. 11(a), the aluminum tubes have four holes drilled and polished on each end of the compression member. Two of the holes are used as the routing path for the cables inside of the rod to come out and connect to the neighboring rods. The two other holes are used for the neighboring cables to connect to.

3D-printed ABS+ Plastic End Caps

One method for reducing friction is to guide the cables out of the hollow aluminum tubes that form the compression members by introducing a smooth contoured surface rather than having the cable travel over the edge of the tube.

The first iteration was made of 3D-printed ABS+ plastic and was modeled relatively simply shown in Fig. 11(b).

(a) (b)

FIGURE 11. (a)CABLE ROUTED DIRECTLY THROUGH POLISHED ALUMINUM TUBE. (b) CABLE ROUTED THROUGH 3D-PRINTED ENDCAP.

Although it served its basic purpose, several flaws existed in the design. The cable still traveled over a relatively sharp angle while exiting the tube. Even though, the design had an exterior fillet that reduced friction effectively, the ABS+ plastic was not resistant to wear which led to the cable wearing channels into the endcaps. These channels increased the cable wear, friction, and prevented the cables from sliding along the circumference of the tube during shape shifting. The off-the-shelf clips used as attachment points for the springs would also frequently tangle with the cables and were inconvenient to attach and detach from the endcap. Also, during punctuated rolling, wear was shown on the endcaps after hours of testing. Lastly, with the elliptical outer geometry, the endcaps seemed to have unpredictable behavior on dirt, sand and other types of rough terrain.

Machined Aluminum Endcap

A new set of aluminum endcaps were designed to address the shortcomings of the 3D-printed plastic endcaps. Machining the next design out of aluminum instead of 3D printing the design addressed the wear problems and reduced the friction by having the cables move on a polished machined surface instead of rougher, 3D printed surfaces. The redesign could be prototyped quickly using standard machine shop tools to maintain the goal of rapid prototyped robot. Due to the unreliability of the off-the-shelf clips for connecting and disconnecting the cables, an inset spring pin was designed as the new attachment system. However, the spring pins did not

function as well as intended. They were meant to be inserted and removed by hand, but due to inconsistencies between pins as well as difficulty creating a hole of the required size for the desired fit, the attempted fits resulted in the pins being too difficult to insert or falling out when tension was released. In addition, a minor sharp edge from one of the milling operation was observed on all endcaps after detailed inspection.

To address the issue of minor sharp edge on the inner wall, the machining method and sequence were adjusted to produce a polished inner wall without defects from machining. In addition, the new design removed the spring pin system and replaced it with two easily machined vertical holes for tying a cable loop for attaching the springs shown in Fig. 12(a). The vertical hole size was adjusted to try different methods of spring attachment shown in Fig. 12(b).

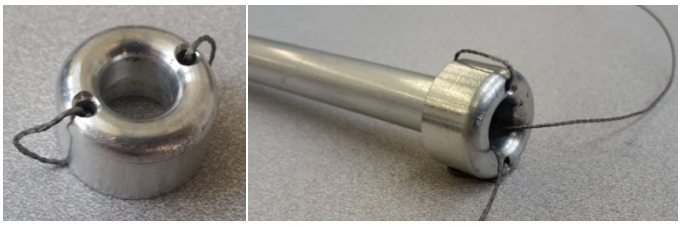

(a) (b)

FIGURE 12. (a)THE MACHINED ALUMINUM ENDCAP. (b) CABLE ROUTED THROUGH THE MACHINED ENDCAP INSTALLED ON THE ALUMINUM TUBE.

Endcap Evaluation

The endcaps were re-designed with the goal of lowering the friction force between the endcap and the cable. This friction delivers a large load on the motors causing them to stall if not handled properly.

An endcap testing platform was developed to quantify the static friction experienced on the cable from the endcap. This testing tool was able to repeatedly test various endcap designs to provide insights on the performance of the designs. With the endcap tester, the baseline performance for the current endcap was established, and used to compare with future iterations.

The endcap was first installed on the tester shown in Fig. 13, then a cable was connected to both scales through the endcap and rod assembly. The turnbuckle was tightened until scale 1 read between 0.5 kg and 1 kg. The cable was pulled away from the endcap and towards scale 2 and then released. This was to ensure there was not a false binding force associated with tensioning the cable. After the readings on each scale were recorded, the turnbuckle was then tightened to a higher tension force, and a new reading was recorded. This process was repeated until nine different tension readings were recorded. When the data collection was finished, the turnbuckle was loosened until the scales again read between 0.5 kg and 1 kg. The process was repeated until there were a total of 4 sets of data per endcap design.

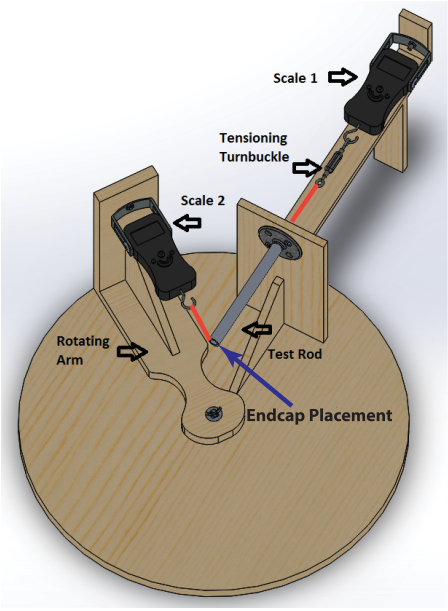

FIGURE 13. 3D MODEL OF THE ENDCAP TESTING PLATFORM.

As seen in Fig. 14, the data revealed an expected linear relationship between the reading on scale 1 and scale 2. The friction force between the cable and the endcap was determined by subtracting the two scale readings. A frictionless endcap would result in no difference between the two readings due to no external forces, so the ideal slope of the data would be 1 with a y-intercept of 0. Therefore, the slope of the line can determine the performance of different endcap designs regarding the friction force between the cable and endcap. The endcaps with high friction forces will have a line with low slope. With this information, the performance of different endcap designs can be ranked.

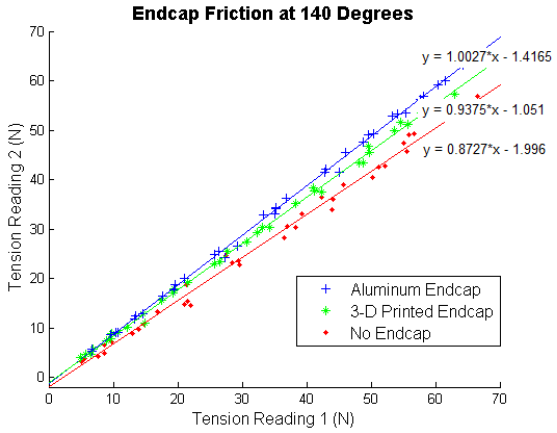

FIGURE 14. PLOT DISPLAYING THE RELATION OF TENSION FORCE ON SCALE 1 AND SCALE 2.

Shown in Fig. 14, the machined aluminum endcap had the least amount of friction between the cable and the endcap,

followed by the 3D-printed ABS+ plastic endcaps. The cable routed through the aluminum rod without an endcap generated the most friction force.

CONTROL AND ACTUATION STRATEGY

The TT-3 robot is based on a six-bar tensegrity structure, which is similar to an icosahedron, a spherical polyhedron. Unlike an icosahedron, the structure is missing six edges on its outer surface, resulting in a total of 24 cables, which form eight equilateral and twelve isosceles triangles. The most natural choice of locomotion for this robot is rolling based on its ball-shaped structure. However, the motion is discontinuous because the robot's outer surface is not perfectly smooth, and therefore this motion is refer to as "punctuated rolling motion." The basic building block of this motion is a "step" which refers to a rotation of the body from one base triangle to another (Fig. 15). The TT-3 robot realizes this step by deforming its body shape by changing the lengths of its member cables in a shape-shifting manner. Not all deformations lead to a step; in order to make a successful step, the deformation should take the ground projection of the center of mass (GCoM) outside of the base triangle.

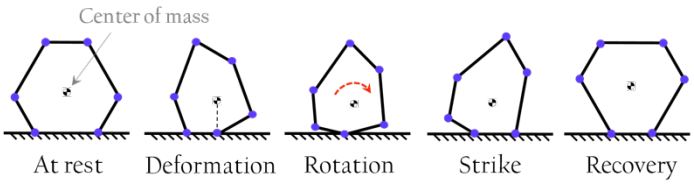

FIGURE 15. A CONCEPTUAL DIAGRAM THAT REPRESENT THE DIFFERENT STAGES OF SHAPE-SHIFTING PERFORMED BY TT-3 TO COMPLETE PUNCTUATED ROLLING.

In previous research, the authors developed actuation policies that resulted in successful performance of punctuated rolling motion for a fully-actuated and cable-driven six-bar tensegrity robot. The search method [17] and multi-generation learning algorithm [8] were used to efficiently handle high dimensional control inputs. The symmetry of the structure was exploited when developing the actuation policies. The policies attempt to achieve two goals with the structure deformation: a) reduce the area of the base triangle, and b) shift the position of GCoM as far as possible from the base triangle to make the structure unstable, thus leading to a step. Depending on the design of the tensegrity robot, multiple cables could be actuated simultaneously to make a step. For example, the TT-2 robot had a rigid linear actuator at the center of each cable edge, and this poses a limitation on the range of cable lengths that could be controlled [17]. As a result, the robot had a limitation on the maximum deformation it could achieve per cable actuation. For this reason, in order to achieve a step, at least three cables required actuation at the same time with the TT-2 robot.

The new design of the TT-3 robot can overcome this barrier. The edges of the TT-3 robot consist of cables and springs without any rigid body components; therefore, there is no mechanical restriction on how much a cable can be retracted, resulting in a greater deformation per actuation when compared to TT-2. In fact, a single cable actuation is sufficient to realize a step with the TT-3 robot. If one of the base triangle cables is fully retracted, the area of the base triangle becomes very small and the structure goes unstable. Hence, no additional actuation is required to shift the position of GCoM away from the base triangle because this will happen as a natural consequence of having a small area base triangle. The direction of a step is determined by which edge of the base triangle is being actuated. There are a total of 3 edges in a triangle; therefore, at each face, there are 3 potential directions of travel shown in Fig. 16. In this work, only the single actuation strategy is implemented on the TT-3 as this is sufficient for the robot to move around on a flat ground. However, when the robot is required to move on uneven terrain (e.g., inclines), greater deformation may be favorable. In this case, the actuation policies developed in the authors' previous work [8,17] will be useful.

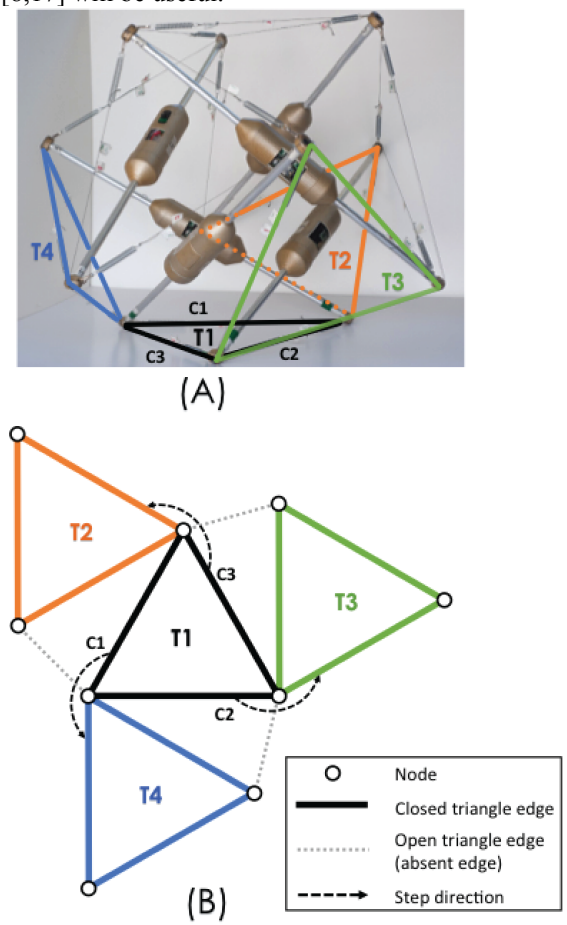

FIGURE 16. (a) A DIAGRAM OF TT-3 WITH LABELED BASED TRAINGLE T1 AND THREE OTHER NEIGHBOR TRIANGLES T2, T3 AND T4. (b) THE DIAGRAM DISPLAYS THE THREE CABLES C1, C2, C3 AND ITS RESULTING TRIANGLE IF ACTUATED. [8,10]

Currently, TT-3 uses wireless communication to signal the actuation commands. Each of the six actuation modules on the tensegrity robot has its own dedicated wireless communication

unit. These wireless communication units act as slave units in the wireless network. The master wireless unit that is used to send commands to the slave unit is placed externally. However, there is no difference between the master and slave units, and any of the slave units can serve as a master, untethering the communication system from external devices. The current communication architecture is chosen for ease of debugging.

With the current control, the desired motor encoder value is sent from the master module to the slave modules. The motor in the slave module will actuate the motor to the desired encoder count, and then send back the updated encoder value when the target is achieved. All 24 motors on TT-3 can be controlled through the method described above.

LOCOMOTION EXPERIMENTS

Various locomotion experiments were performed to observe the behavior of the robot. The first test for the robot was to roll in a circular trajectory. The robot was able to successfully roll in a circular pattern continuously on flat ground. The robot only required four steps to complete a full circle, and was able to roll continuously with a single actuation module.

The second test on the robot was to walk in a straight trajectory. It was able to accomplish the straight line-walk in a punctuated rolling style on a flat concrete floor shown in Fig. 17. The measured rolling velocity was 5 cm/s for TT-3.

FIGURE 17. TT-3 PERFORMING STRAIGHT LINE WALK.

The third experiment on the robot was to perform punctuated rolling in a straight line while carrying a simulated payload at the center of the robot. This experiment helps the authors to visualize the interaction between the payload and the robot during locomotion. Figure 18 shows the steps performed by TT-3 while carrying a payload at the center of the robot. The payload did not interfere with the shape shifting required for a step during the experiment.

FIGURE 18. TT-3 PERFORMS STRAIGHT LINE WALK WHILE CARRYING A CENTER PAYLOAD.

In addition to the indoor tests, TT-3 was tested to roll on an uneven outdoor terrain. Not surprisingly, it appeared to be more difficult for the robot to roll on loose dirt than flat concrete floor. The rods of the robot seem to dig into the dirt or drag along the dirt during punctuated rolling. However, the robot was successful in performing the straight line roll command.

FIGURE 19. TT-3 PERFORMS STAIGHT LINE WALK ON AN UNEVEN OUTDOOR TERRAIN.

CONCLUSION AND FUTURE RESEARCH

TT-3, a six-bar tensegrity robot, has been demonstrated in this paper to be an effective mobile robot that can sustain impact. The robot was able to continuously roll in a circle with a single active actuation module and in a straight-line trajectory with three active actuation modules, with and without a payload at the center. For space missions we envision this payload containing sensors, spectrometers, cameras or other light-weight scientific equipment. Base on its compliant nature, there are other potential co-robotic applications for TT-3. For instance, TT-3 can be envisioned to as a medicine transport robot in a hospital environment. Due to its intrinsic compliance, the robot will not injure humans, which is one of its most important features.

Furthermore, the rod-centered design has shown to improve the system's ability to absorb impact, and minimize the damage to the critical components like actuators and controllers. Although it has been shown that the TT-3 robot can absorb and dissipate energy during impact by greatly deforming its shape, the collision of the rods with each other during deformation has not been explicitly tested. From some preliminary physical hardware testing, it was shown that the TT-3 robot was not damaged by rod collision, but more elaborate analyses and experiments should be done in order to guarantee the robustness of the robot. In the future, impact tests with systematically changing physical parameters (e.g., pretension) to characterize the behavior of the robot under different impact conditions will be performed. Such tests will allow for optimization of the robot's design parameters that can best survive from significant impact.

A current challenge with the robot is the lack of feedback control. The robot must be autonomous in order to successfully execute space missions where human supports are limited. This requires a high-level feedback controller as well as sensors to gather information about surroundings. The TT-3 robot does not have any functional sensors at this point, but we are in the process of integrating and testing different types of sensors such as inertial measurement units. Furthermore, a better performance control algorithm is under development that will allow the robot to move on uneven terrain.

ACKNOWLEDGMENTS

The authors are grateful for funding support from NASA's Early Stage Innovation grant NNX15AD74G. We also wish to acknowledge the work of the graduate and undergraduate student working on this project: Azharuddin Khaderi, Alexander Lim, Peadar Keegan, Deaho Moon, ChanWoo Yang, Raymond Ennis, Wesley Wang, Vincent Donato, and Jeremy

Wan. In addition, we thank Andrew Sabelhaus, Kyle Zampaglione, Thomas Clark and Colin Ho for their valuable feedback on design options,

REFERENCES

[1] B. Fuller, "Tensegrity," in *Portfolio and Art News Annual*, vol. 4, pp. 112–127, 1961.

[2] R. Skelton, R. Adhikari, J. Pinaud, W. Chan, J. W. Helton, "An introduction to the mechanics of tensegrity structures." Decision and Control, 2001. Proceedings of the 40th IEEE Conference on. Vol. 5. IEEE, 2001.

[3] K. Snelson. (2013). *Kenneth Snelson, Art and Ideas* [Online]. Available: http://kennethsnelson.net/KennethSnelson_Art_And_Ideas.pdf

[4] G. Tibert, "Deployable Tensegrity Structures for Space Applications," Ph.D. dissertation, Dept. Mech., Royal Inst. Of Tech., Stockholm, Sweden, 2002.

[5] F. Feng, "Structural behavior of design methods of Tensegrity domes," in *Journal of Constructional Steel Research,* vol. 61, iss. 1., pp. 22-35, 2005.

[6] A. P. Sabelhaus, J. Bruce, K. Caluwaerts, P. Manovi, R.F. Firoozi, S. Dobi, A. M. Agogino, V. SunSpiral, "System Design and Locomotion of SUPERball, an Untethered Tensegrity Robot," in IEEE 2015 International Conference on Robotics and Automation, Seattle, WA., 2015.

[7] K. Caluwaerts J. Despraz, A. Iscen, A. P. Sabelhaus, J. Bruce, B. Schrauwen, V. SunSpiral, "Design and control of compliant tensegrity robots through simulation and hardware validation," in *Journal of the Royal Society Interface*, vol. 11, iss. 98, 2014.

[8] K. Kim, A. K. Agogino, A. Toghyan, D. Moon, L. Taneja, A. M. Agogino, "Robust learning of tensegrity robot control for locomotion through form-finding," in IEEE 2015 International Conference on Intelligent Robots and Systems, Hamburg Germany, 2015.

[9] J. Friesen, A. Pogue, T. Bewley, M. D. Oliveira, R. Skelton, V. SunSpiral, "DuCTT: a Tensegrity Robot for Exploring Duct Systems," in IEEE 2014 International Conference on Robotics and Automation, Hong Kong, China, 2015.

[10] B. Mirletz, I. Park, T. Flemons, A. K. Agogino, R. D. Quinn, V. SunSpiral, "Design and Control of Modular Spine-Like Tensegrity Structures," in The 6th World Conference of the International Association for Structural Control and Monitoring, Barcelona, Spain, 2014.

[11] A. P. Sabelhaus, H. Ji, P. Hylton, Y. Madaan, A. M. Agogino, J. Friesen, V. SunSpiral, "Mechanism Design and Simulation of the ULTRA Spine: A Tensegrity Robot," in the ASME 2015 International Design Engineering Technical Conferences & Computers and Information in Engineering Conference, Boston, MA, 2015.

[12] J. Friesen, M. Fanton, P. Glick, P. Manovi, A. Xydes, T. Bewley, V. SunSpiral, "The Second Generation Prototype of A Duct Climbing Tensegrity Robot, DuCTTv2″, To appear in proceedings of 2016 IEEE International Conference on Robotics and Automation, (ICRA2016), May 2016, Stockholm, Sweden.

[13] L. Rhode-Barbarigos, "An Active Deployable Tensegrity Structure," Ph.D. dissertation, Dept. Struct. Engr., Ecole Polytechnique Fédérale de Lausanne, Lausanne, Switzerland, 2012.

[14] C. Paul, F. J. Valero-Cuevas, H. Lipson, "Design and Control of Tensegrity Robots for Locomotion," in *IEEE Transactions on Robotics*, vol. 22, no. 5, 2006.

[15] C. Paul *et al.,* "Gait Production in a Tensegrity Based Robot," in The 12th International Conference on Advanced Robotics, Seattle, WA, 2005.

[16] NTRT - NASA Tensegrity Robotics Toolkit. (n.d.). Date Tested June 15, 2015, from http://ti.arc.nasa.gov/tech/asr/intelligent-robotics/tensegrity/NTRT/

[17] Kyunam Kim, Adrian K. Agogino, Deaho Moon, Laqshya Taneja, Aliakbar Toghyan, Borna Dehghani, Vytas SunSpiral, and Alice M. Agogino. "Rapid prototyping design and control of tensegrity soft robot for locomotion." In Robotics and Biomimetics (ROBIO), 2014 IEEE International Conference on, pp. 7-14. IEEE, 2014.